Journal of Applied Electrochemistry **30**: 625–634, 2000.

Faradaic impedance investigation of the deactivation mechanism of Ir-based ceramic oxides containing TiO_2 and SnO_2

T.A.F. LASSALI[1*], J.F.C. BOODTS[2] and L.O.S. BULHÕES[3]
[1]*Depto de Física e Matemática, FFCLRP/USP, Av. Bandeirantes 3900, 14040-901, Ribeirão Preto – SP, Brazil;*
[2]*Depto de Química, Universidade Federal de Uberlândia, Campus Santa Mônica, Av. João Naves De Avila 2160, 38400-902, MG, Brazil;*
[3]*Depto. de Química, Universidade Federal de São Carlos/UFScar, Rodovia Washington Luiz km 235, C.P. 676, 13565-905, São Carlos, SP, Brazil*
*(*author for correspondence, Fax: +55-16-633-9949; E-mail: tlassili@usp.br)*

Received 18 August 1999; accepted in revised form 5 January 2000

Key words: deactivation mechanism, impedance faradaic spectroscopy, iridium dioxide, tin dioxide

Abstract

Ti-supported $IrO_2/SnO_2/TiO_2$ coatings were prepared by thermal decomposition of the chloride precursor mixtures (400 °C). The effect of the replacement of TiO_2 by SnO_2 on the service life of the $Ti/IrO_2 + TiO_2$ coating was investigated under galvanostatic polarization at 0.8 A cm^{-2} in 1.0 mol dm^{-3} $HClO_4$. The deactivation mechanism of the electrodes, using OER as the reaction model, was investigated through the periodic recording of voltammetric curves (VC) and impedance spectra (EIS) as a function of the anodization time. Bulk composition and morphology of the electrode coatings were investigated by energy dispersive X-ray (EDX) and scanning electron microscopy (SEM) before and after accelerated life tests. The service life showed a dependence on the electrode composition. Replacement of TiO_2 by SnO_2 in the $Ir_{0.3}Ti_{0.7}O_2$ electrode led to a decrease in the service life of these systems above 30% mol SnO_2 content. This behaviour is directly related to morphological factors and the absence of synergetic effects. The behaviour of the parameters supplied by the EIS, VC, SEM, and EDX analyses made it possible to describe the overall deactivation mechanism.

1. Introduction

Dimensionally stable anodes, DSA®, based on IrO_2 are frequently adopted as electrocatalytic material for O_2 evolution in acid medium, due to their high activity and stability against anodic corrosion. This oxide is a natural choice from the technological point of view for the replacement of the RuO_2 in DSAs, because both possess the smallest overpotential for OER of any of the platinum metals. Furthermore, it has the advantage over RuO_2 of being stable at potentials above 1.85 V/RHE, potential at which, RuO_2 already presents a quite significant corrosion rate [1, 2]. The stability of the IrO_2-based electrodes has also been investigated from the point of view of the base metal used and the oxide added as the modulator agent [3, 4]. The adoption of tantalum as the base metal increased the service life of the electrode containing IrO_2 as the active component for the OER [4]. The effect of coating thickness and surface treatment on the titanium base metal was recently studied by Krýsa et al. [5, 6].

The aim of this research is to analyse the effect of the replacement of TiO_2 by SnO_2 on the service life of the $Ti(Ir + Ti)O_2$ coating. The deactivation mechanism of the electrodes, using OER as the reaction model, was investigated by periodically recording the voltammetric curves and impedance spectra as a function of the anodization time at high current density (0.8 A cm^{-2}).

2. Experimental

2.1. *Electrode preparation*

A series of eight electrodes with a $Ir_{0.3}Ti_{(0.7-x)}Sn_xO_2$ ($0 \leq x \leq 0.7$) nominal composition was prepared, starting with a $Ir_{0.3}Ti_{0.7}O_2$ composition. The mol content of IrO_2 was kept constant, while SnO_2 replaced TiO_2 in 10% mol steps. The oxide layers were prepared by thermal decomposition (T_{calc}: 400 °C; O_2 flux: 5 L min^{-1}; t_{calc}: 1 h), of 0.18 mol dm^{-3} of $TiCl_4$ (Aldrich), $IrCl_3.xHCl.yH_2O$ (Aldrich) and $SnCl_2.2H_2O$ (Vetec) mixtures dissolved in HCl 1:1 (v/v), used as precursor solutions. The experimental conditions for the precursor solutions and electrode preparation were described previously [7].

The nominal coating thickness was kept constant at 2 μm corresponding to between 2.02 and 3.70 mg oxide

loading (depending on composition). Electrode mounting and further details are given elsewhere [8].

2.2. *Techniques and experimental procedure*

The electrochemical surface characterization of the mixed oxide electrodes was accomplished by means of voltammetric curves recorded at 20 mV s^{-1} between 0.4 and 1.4 V/RHE (reversible hydrogen electrode) in 1.0 mol dm^{-3} $HClO_4$ solution. After measurement of the open circuit potential, E_{oc}, the electrodes were submitted to continuous cycling of the potential for 50 cycles, until a steady surface state was reached. The impedance spectra of the system were recorded at constant potentials (1.475, 1.50 and 1.525 V/RHE) located in the OER domain.

The stability against anodic corrosion was evaluated under galvanostatic conditions at a high current density (0.8 A cm^{-2}) in 1.0 mol dm^{-3} $HClO_4$, recording the electrode potential as a function of time. The service life for a given electrode was determined by the time at which the anode potential reached 6 V/RHE. Above this value the electrode was considered inactive for OER. The *E–t* curve was interrupted at regular intervals to record the voltammetric curve and the impedance spectra at the values of the potentials mentioned. All electrochemistry experiments were repeated twice.

The bulk composition and morphology of the electrode coatings were investigated by energy dispersive X-ray (EDX) and scanning electron microscopy (SEM) before and after accelerated life tests. Experimental conditions of EDX analysis were adjusted, so that a thickness of about 0.6 μm is analysed.

2.3. *Equipment*

The voltammetric curves and accelerated life test were performed with a potentiostat–galvanostat model 273 from EG & G Princeton Applied Research (PAR), coupled to an IBM PS/2 microcomputer model 55SX, and monitored by the M270 PAR software. In the studies of electrochemical impedance spectroscopy (EIS), the potentiostat was coupled to a Lock-in Amplifier (LIA) PARC model 5210. EIS measurements were obtained using the PARC M388 computer program covering the frequency interval of 100 kHz–5 MHz, with a sine wave amplitude of 5 mV (p/p). The experimental impedance spectra were interpreted based on an equivalent circuit using the EQUIVCRT program elaborated by Boukamp [9].

The bulk composition and morphology of electrode coatings were investigated by EDX and SEM using a Zeiss model DSM 960 microscope connected to a LINK ANALYTICAL model QX 2000 microanalyzer. A four-compartment cell [10] was used in all experiments. Electrode potentials are reported against the RHE scale.

3. Results and discussions

3.1. *E vs. t curve behaviour*

Figure 1 shows representative chronopotentiometric curves of the $IrO_2/TiO_2/SnO_2$ system as function of the composition submitted to a current density of 0.8 A cm^{-2} in 1.0 mol dm^{-3} $HClO_4$. Independent of the composition, these curves are characterized for a very slow variation of the potential, with the anodization time followed by an abrupt increase in this value around 6 V/RHE at the end of the service life of the electrode.

The $Ir_{0.3}Ti_{0.7}O_2$ electrode showed an average service life of 15 h. Considering the value of the deposited mass of IrO_2, this system showed an experimental dissolution speed of approximately 4.7×10^{-5} g cm^{-2} h^{-1}. Different service life values have been cited in the literature for systems containing IrO_2 as the electrocatalytic component for the OER. A direct comparison of these different values should be made with extreme caution, because differences in the parameters such as, the value of the applied current density, oxide layer composition, oxide layer thickness, thermal treatment temperature, nature of the precursor and solvent, and the nature of the metallic support are all considered of great importance for the stability of the oxide layer.

Service life values much larger than those observed in this work have been cited in the literature. Under the same experimental conditions, the $Ir_{0.3}Ti_{0.7}O_2$ electrode prepared at 450 °C [11] showed a service life 3 times larger than that observed for the oxide layer prepared at 400 °C. This result is in agreement with that observed in the literature when the calcination temperature of the oxide layer is varied [12]. The longer service life appears to be a consequence of an increase in the degree of crystallization of the constituent oxides and the reduction of the surface area (increasing the protection of the metallic base against passivation) [13]. The service life of

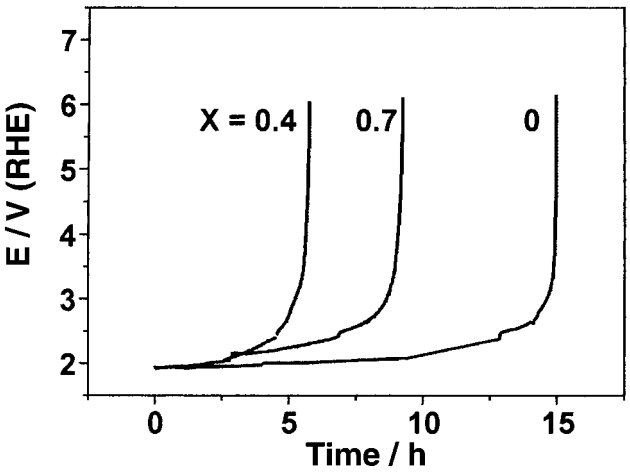

Fig. 1. Representative potential – time curves as function of the nominal composition of $Ir_{0.3}Ti_{(0.7-x)}Sn_xO_2$ electrodes in 1.0 mol dm^{-3} $HClO_4$. $j = 0.8$ A cm^{-2}.

$IrO_2/RuO_2/TiO_2$ as function of composition electrodes varied from 0.8 to 560 h confirming the decisive influence of the oxide layer composition on the service life of a system [14].

The introduction of the third component in the IrO_2/TiO_2 system did not produce significant changes in the value of the initial potential of the E–t curve, suggesting no change in the overall electrocatalytic performance of the system (inset Figure 2). However, the replacement of TiO_2 by SnO_2 led to a decrease in the service life of these electrodes, with lower performance for electrodes with SnO_2 content >30% mol (Figure 2). The effective current density applied to the electrodes as a function of the oxide layer composition is shown in Figure 3. A decrease in the effective current density is observed for SnO_2 contents $\geq$30% mol. So, contrary to the experimentally observed values one would expect an increase in service life.

The decrease in the deactivation time of the electrodes, promoted by the introduction of SnO_2, may have at least two different causes: (a) the presence of SnO_2 hindered the formation of a solid solution between IrO_2 and TiO_2, hampering the stabilizing action of TiO_2 on the active component thus facilitating the deactivation of the oxide layer by mechanisms such as erosion and/or corrosion; (b) the increase in the electroactive area of these anodes, promoted by the introduction of SnO_2, supported by both the q_a-values and SEM micrographs, may have facilitated the metal base passivation. The passivation phenomenon may be facilitated by solution penetration through pores and cracks reaching more easily the metallic support. Further support for metal base passivation as a possible cause of high area electrode deactivation is obtained from the EDX data (see Figure 13e, f) which show that the high area Ti/$Ir_{0.3}Sn_{0.7}O_2$ electrode, once deactivated, still presents a high Ir-content.

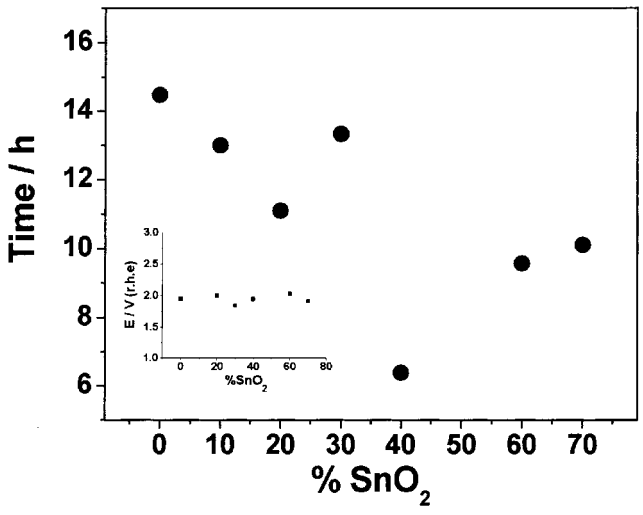

Fig. 2. Service life as a function of the nominal composition of the $Ir_{0.3}Ti_{(0.7-x)}Sn_xO_2$ electrodes in 1.0 mol dm^{-3} $HClO_4$ at 0.8 A cm^{-2}. Values are the average of duplicate experiments. *Inset*: Variation of the initial cell potential (E_{cell}) with the nominal composition.

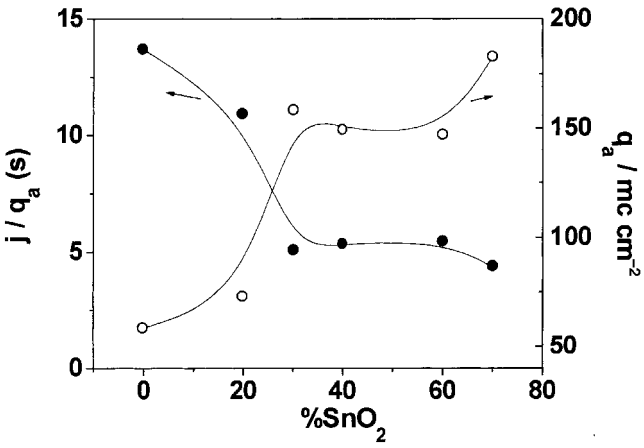

Fig. 3. Effective current density, j/q_a, applied to the electrodes and values of the anodic voltammetric charge (q_a) as a function of the nominal SnO_2 content.

The possibility of item (a) being one of the causes of the deactivation mechanism is corroborated by the fact that the nominal composition of these electrodes is different from the nominal value [7]. Due to the high volatility of the Sn precursor, the IrO_2 content is progressively greater in the oxide layer, while the amount of TiO_2 removed from the system is not completely replaced by SnO_2. After total replacement of TiO_2, the resulting oxide layer has ~70% mol of IrO_2. Although the Ti/IrO_2 electrode has high catalytic activity it does not show high mechanical stability requiring a stabilizing agent to improve its physical properties.

3.2. *Study of the deactivation mechanism by cyclic voltammetry*

The voltammetric behaviour of the $IrO_2/TiO_2/SnO_2$ system as a function of composition, before and after the accelerated life tests, is shown in Figure 4. Independent of the SnO_2 content, the voltammetric curves are characterized by the presence of the Ir^{+3}/Ir^{+4} solid state redox transition, suggesting that the electrochemistry of the surface of this system is controlled by this component. E_{oc} values close to 0.92 V/RHE corroborate these results. The introduction of SnO_2 produced an increase in the surface area of the electrodes (Figure 3). This increase in surface area may be attributed to the formation of a finely divided oxide layer, due to the lower degree of interaction between the different oxide components. This result was confirmed by SEM analyses of the freshly prepared electrodes.

The deactivation of the electrodes was accompanied by periodic recording of voltammetric curves, with the goal of monitoring changes in the surface provided by the continuous anodization. Figure 5 shows the variation of the cyclic voltammograms as a function of the service live of the $Ir_{0.3}Ti_{0.3}Sn_{0.4}O_2$ electrode as representative of the system behaviour. Independent of the service life, the cyclic voltammogram showed the

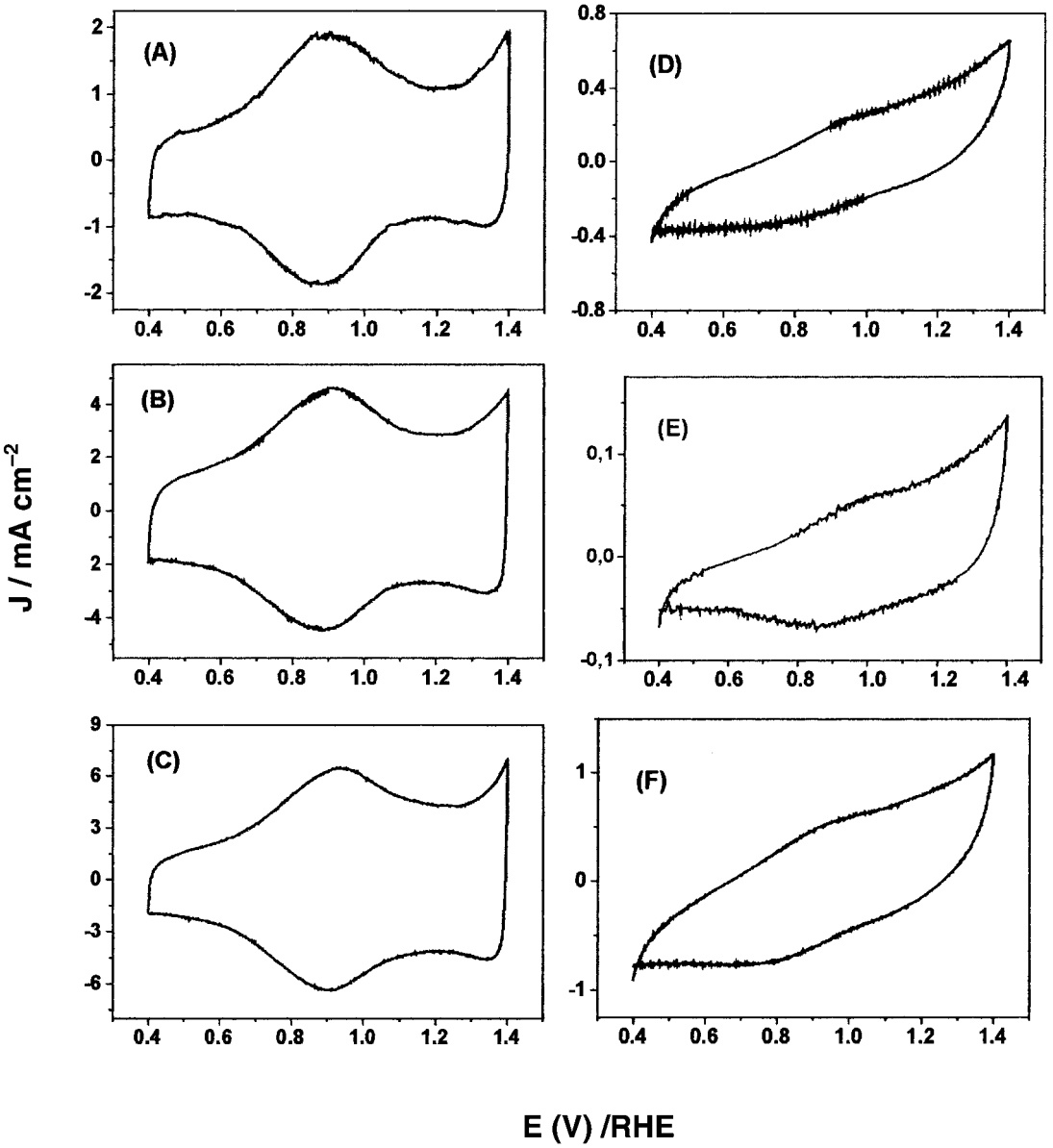

Fig. 4. Cyclic voltammograms of freshly prepared electrodes (a, b, and c) and after accelerated test life (d, e, and f) in 1.0 mol dm^{-3} $HClO_4$; 20 mV s^{-1}. Nominal electrode composition: $Ir_{0.3}Ti_{(0.7-x)}Sn_xO_2$. (a) and (d) $x = 0$; (b) and (e) $x = 0.4$; (c) and (f) $x = 0.7$.

Ir^{+3}/Ir^{+4} surface transition. Even after total deactivation of the oxide layer (a condition assumed after the potential electrode reaches 6 V/RHE), the voltammetric curves still presented evidence of this redox process, suggesting a residual IrO_2 content is still present in the oxide layer. Comparing the initial voltammetric charge with the charge obtained at the end of the service life, active oxide surface contents between 3–10% mol were calculated. These results are in agreement with the analyses of EDX, which confirm the presence of Ir after deactivation of the oxide layer. Krýsa et al. [15] found, investigating the effect of the coating thickness on the electrochemical properties of Ti/IrO_2-Ta_2O_5, a relationship between Ir content of the oxide layer and the service life. These authors estimated that the minimum amount of Ir to sustain oxygen evolution with low overpotential is about ~0.06 mg Ir cm^{-2}. The values of the 0.08–0.009 mg Ir cm^{-2} calculated by us for the $Ir_{0,3}$-$Ti_{(0.7-x)}Sn_xO_2$ electrodes after deactivation are in good agreement with the value reported by Krýsa et al. [15]. The rather broad range of residual Ir-content observed is due to the fact that for the high surface electrodes, passivation of the metal support is the main cause of electrode deactivation (see item 3.4) and occurs when significant amounts of IrO_2 are presents.

Figure 6 shows the behaviour of the anodic voltammetric charge, q_a, as a function of the anodization time for $Ir_{0.3}Ti_{(0.7-x)}Sn_xO_2$ electrodes. In general, the greater the anodization time the smaller the q_a value, suggesting that the continuous loss of electroactive material contributes to the deactivation mechanism in most of the electrodes. In RuO_2-based systems, this behaviour is attributed to the oxidation of the Ru(IV) active sites to higher oxidation states when potentials above 1.5 V/RHE are reached [16, 17]. RuO_2 present in the oxide layer can be lost as volatile RuO_4 or as H_2RuO_5,

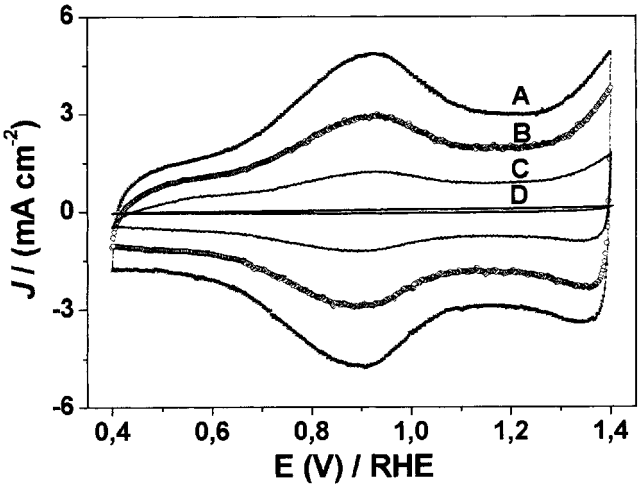

Fig. 5. Cyclic voltammograms of $Ir_{0.3}Ti_{0.3}Sn_{0.4}O_2$ electrode as function of anodization time at 0.8 A cm^{-2}. 1.0 mol dm^{-3} $HClO_4$, 20 mV s^{-1}. (a) 0, (b) 2, (c) 7, and (d) 9 h.

soluble in acid solution. The formation of soluble Ir species, such as $IrO_4^=$, at potentials higher than 2.0 V/RHE has been mentioned in the literature for IrO_2 films anodically grown on Ir metal [18, 19].

Analysis of the E/t curves (Figure 1) shows two potential behaviours can be distinguished in the potential region before electrode deactivation: (a) the time interval where $E \approx 2$ V is related with to elimination of the more porous oxide region due to erosion combined with corrosion; (b) the time interval where $E > 2.5$ V is related to the destruction due to corrosion of the more compact oxide region. Near the end of the service life passivation of the Ti-support contributes to the deactivation of the electrode. This behaviour is consistent with the q_a vs. service life curves (Figure 6) and SEM (Figure 12) results.

3.3. *Study of the deactivation mechanism by EIS*

With the aim of evaluating the deactivation mechanism of $IrO_2/TiO_2/SnO_2$ electrodes periodic impedance measurements were performed during the life tests under accelerated conditions. Nyquist diagrams as a function of anodization time are shown in Figures 7 and 8 for electrodes having 0 and 70% SnO_2 content (1.475 V/RHE). Before the start of the accelerated life test ($t = 0$ h), the impedance spectra are characterized in the low frequency domain by a well defined semi-circle related to the kinetic parameters of the OER while at high frequencies a behaviour is observed which is dependent on the applied potential.

A detailed investigation of the dependence of the impedance spectra on applied potential was done earlier [20]. For the less positive potential values ($E < 1.475$ V), the high frequency region of these spectra does not present a well-defined semi-circle but rather a straight line, or the beginning of the formation of a semi-circle. For more positive potentials ($E \geq 1.475$ V), the behaviour of the impedance spectrum at high frequencies assumes the aspect of a semi-circle, independent of the composition of the oxide layer. Lassali et al. [12] concluded that the response in the high values frequency domain of EIS is governed by threshold values of the porosity/rugosity of the near to the surface oxide region

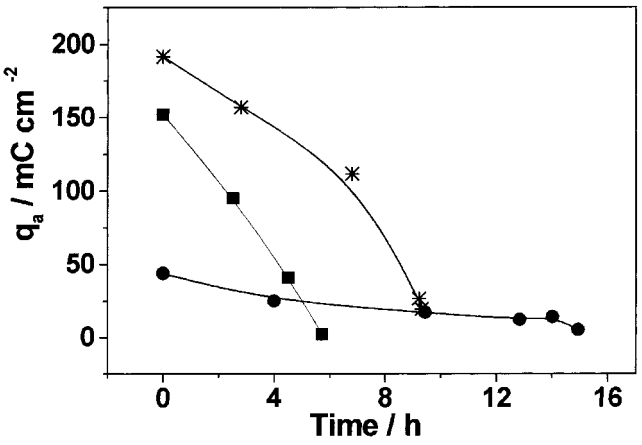

Fig. 6. Anodic voltammetric charge, q_a, as a function of service life of $Ir_{0.3}Ti_{(0.7-x)}Sn_xO_2$ electrodes in 1.0 mol dm^{-3} $HClO_4$ at 0.8 A cm^{-2}, (●) $x = 0$; (■) $x = 0.4$; (∗) $x = 0.7$.

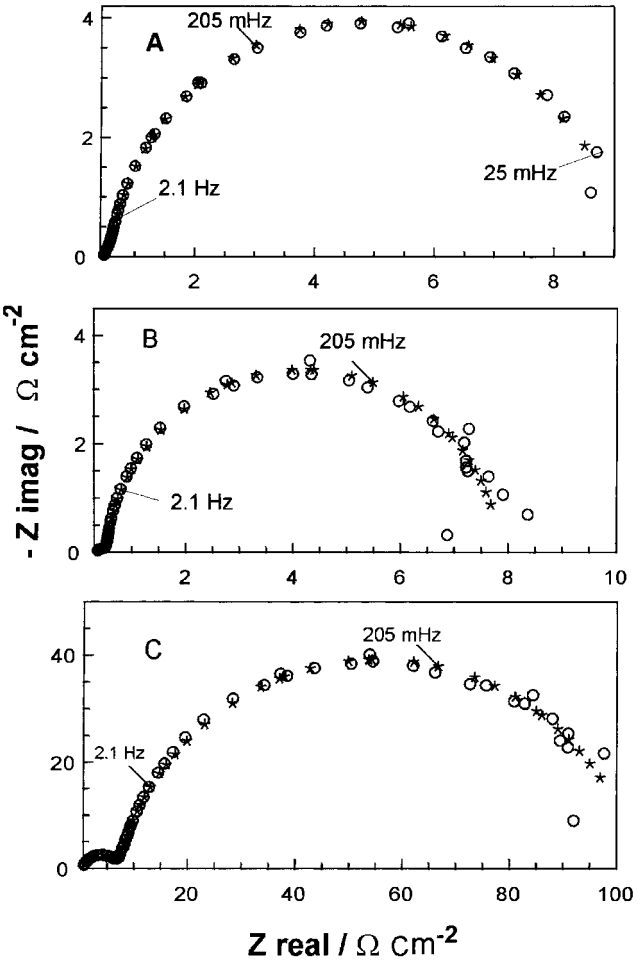

Fig. 7. Nyquist diagrams as a function of the anodization time of $Ir_{0.3}Ti_{0.7}O_2$ electrodes in 1.0 mol dm^{-3} $HClO_4$ at 0.8 A cm^{-2}. $E = 1.475$ V/RHE. (a) 0, (b) 4, and (c) 15 h. (○) Experimental, (+) simulated data.

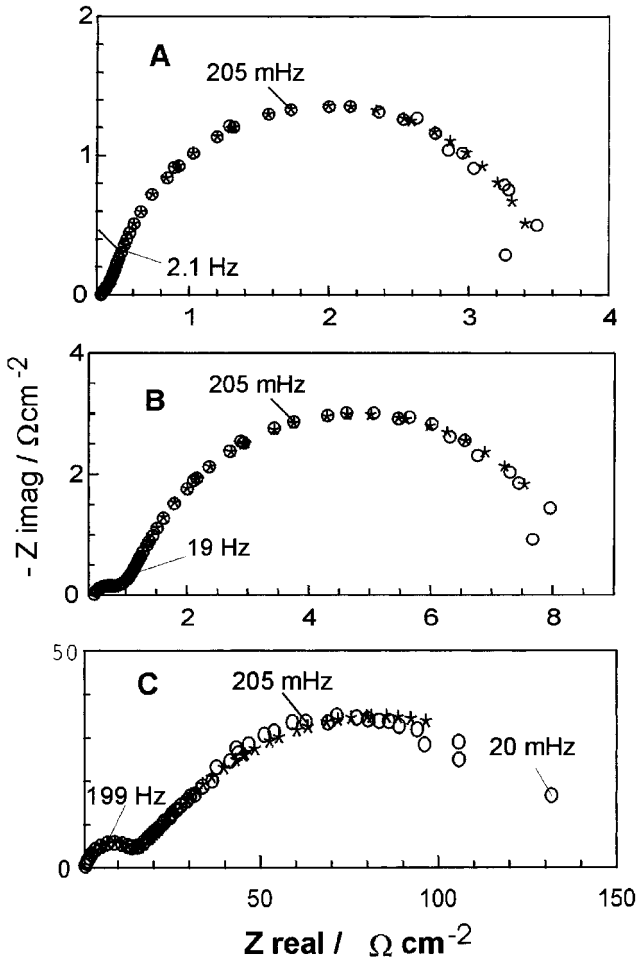

Fig. 8. Nyquist diagrams as a function of the anodization time of $Ir_{0.3}Sn_{0.7}O_2$ electrodes in 1.0 mol dm^{-3} $HClO_4$ at 0.8 A cm^{-2}. $E = 1.475$ V/RHE. (a) 0, (b) 7, and (d) 9 h. (○) Experimental, (+) simulated data.

and the conductivity of the $TiO_2(Ti_2O_3)$ interlayer at the Ti°-support/bulk oxide interface formed during electrode preparation.

Independent of the applied potential, the impedance spectrum in the high frequency region is dependent on the anodization time. The greater the anodization time the more this spectral region assumes the shape of a semi-circle (see Figures 7 and 8). These results suggest that under severe anodic conditions the TiO_2/Ti_2O_3 film formed between the metal base and the conductive oxide layer in the electrode preparation stage tends to grow with the anodization time thus increasing the film resistance. This result is in agreement with the CV, which indicates a resistive element as revealed by the rather sluggish current change observed at E_λ. Similar results have been obtained by Alves et al. [11] for the anodic polarization of Ti/(Ir + Ti)O_2 electrodes at 0.4 A cm^{-2} in 1.0 mol dm^{-3} $HClO_4$. The growth of this film with time and with potential has also been observed by Loucka [21].

Before the beginning of the accelerated life test, the TiO_2/Ti_2O_3 film contributes little to the ohmic resistance of the system, probably due to the solubility of the IrO_2 catalyst in TiO_2 leading to the formation of an efficiently IrO_2-doped TiO_2/Ti_2O_3 film [22]. Oxidation processes of Ti° to higher oxidation states already occur at negative potentials (e.g. Ti/TiO; $E_o = -1.306 - 0.0591$ pH). At the positive working electrode potentials (+2 V) the charged species necessary to balance the Ti^{+4} species are furnished through an O^{-2} "hopping" mechanism. As a result undoped TiO_2 starts growing, increasing in thickness during the execution of the service life tests.

$$Ti_{metallic} \longrightarrow Ti^{+4} + 2O^{=} \rightarrow TiO_2 \qquad (1)$$

This process progressively leads to a decrease in the conductivity of the TiO_2/Ti_2O_3 interlayer, generating the capacitive behaviour observed at the high frequencies in the impedance spectrum. The greater the anodization time the higher the resistance of this film and the better the definition of the semi-circle observed in the high frequency range of the spectrum.

The equivalent circuit which best fits the experimental EIS data is a $R_\Omega(R_fC_f)(R_{ct}C_{dl})$ combination (Figure 9), with (R_fC_f) accounting for the behaviour of the TiO_2 interlayer (Ti-support/active oxide layer interface), formed during electrode preparation, in series with a $(R_{ct}C_{dl})$ combination to describe the OER at the active layer/solution interface.

Independent of composition and anodization time, R_Ω-values between 0.3–0.5 Ω were found, which are consistent with the conductive properties of the supporting electrolyte used. For freshly prepared electrodes, and during most of its service life, $R_\Omega > R_f$, though the latter increases progressively. These results not only show that the contribution of the IrO_2-doped TiO_2 interlayer to the ohmic resistance of the system is small, but also suggest that the oxidation of the Ti-support, resulting in poorly doped TiO_2, is slow during most of the anodization experiment, especially for TiO_2-rich electrodes.

The behaviour of R_f and C_f with the anodization time is shown in Figure 10 at $E = 1.475$ V as a function of composition. For 0–60% SnO_2 content, R_f increases more quickly near the end of the service life, rising rapidly when the electrode is totally deactivated (the E_{cell} increases abruptly to 6 V/RHE). This behaviour suggests that the oxidation of the Ti metal base is the main cause of total deactivation of the electrode material only near the end of the service life. The faster increase of R_f during most of the service life observed for SnO_2-rich electrodes

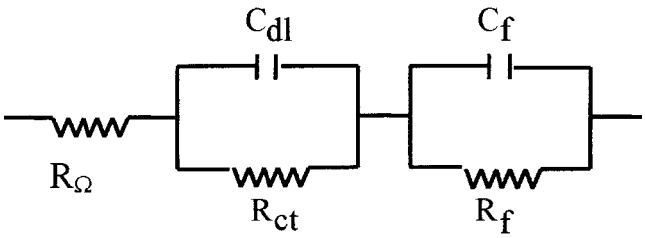

Fig. 9. Equivalent circuit used in the simulation of the experimental results. The description of the circuit follows Boukamp's notation [9].

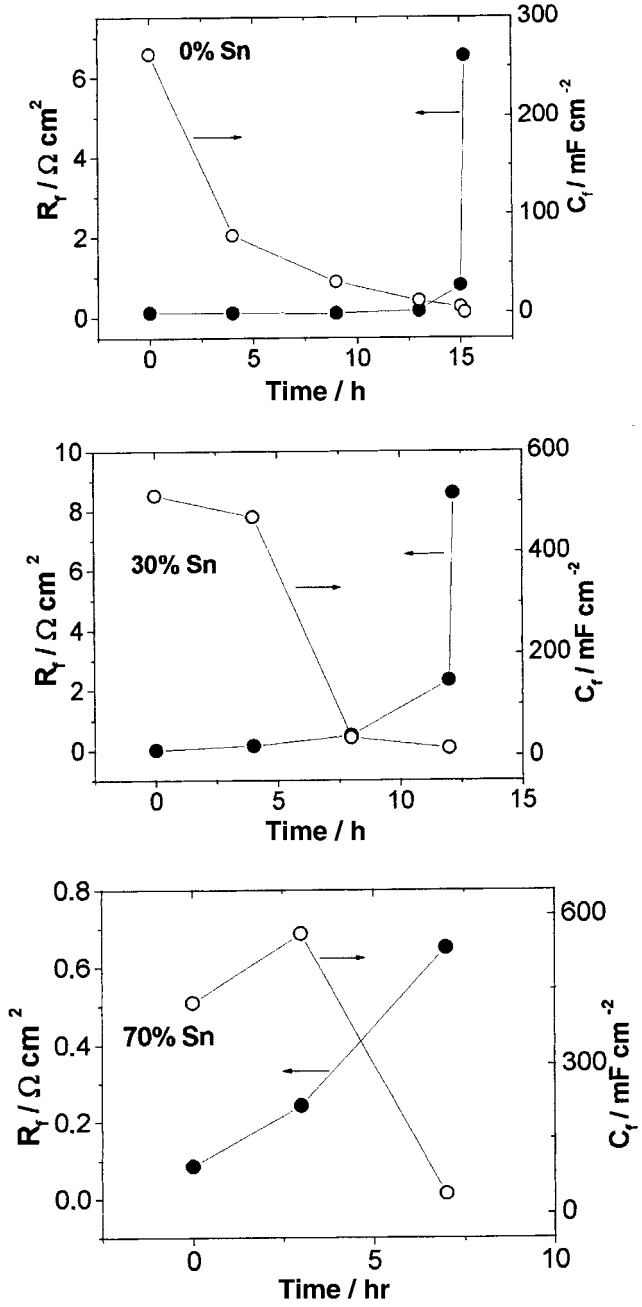

Fig. 10. R_f and C_f as a function of the anodization time of $Ir_{0.3}Ti_{(0.7-x)}Sn_xO_2$ electrodes in 1.0 mol dm^{-3} $HClO_4$ at 0.8 A cm^{-2}. $E = 1.475$ V/RHE.

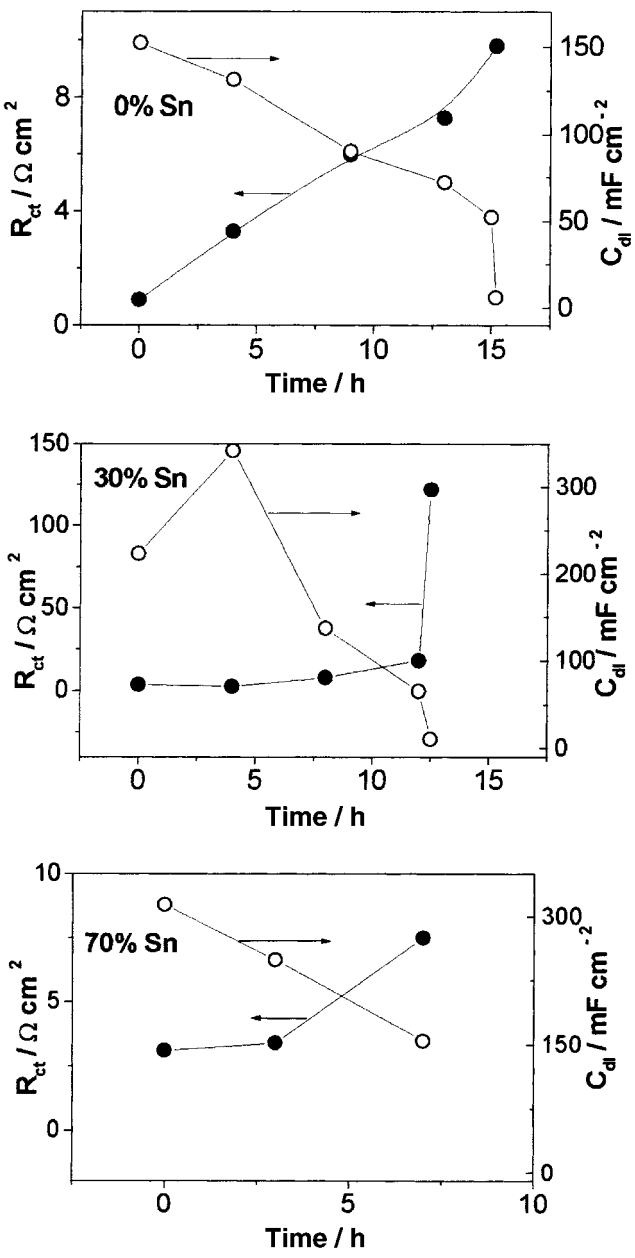

Fig. 11. R_{ct} and C_{dl} as a function of the anodization time of $Ir_{0.3}Ti_{(0.7-x)}Sn_xO_2$ electrodes in 1.0 mol dm^{-3} $HClO_4$ at 0.8 A cm^{-2}. $E = 1.475$ V/RHE.

suggests a larger contribution of passivation to the deactivation process under these conditions. This behaviour may be related to the high surface area presented by these electrodes (60–70% SnO_2 – see Figure 3).

The R_f behaviour supports, and is consistent with, the C_f-values, which gradually decrease during most of the service life, showing a sharp decrease when the total deactivation of the electrode occurs.

Figure 11 shows the variation of C_{dl} and R_{ct} with anodization time ($E = 1.475$ V) for electrodes with different SnO_2 contents. Similarly to the q_a behaviour, during anodization the C_{dl}-values decrease gradually with an abrupt change at the end of the experiment. This behaviour suggests that the surface area slowly decreases due to gradual loss of the electroactive material, probably through the combination of phenomena such as erosion and corrosion, the electrode gradually exposing a more compact surface to the solution.

Except for the $Ir_{0.3}Ti_{0.7}O_2$ electrode, R_{ct}-values remain almost constant during most of the anodization experiment with an abrupt change occurring on deactivation of the electrode material. The behaviour is evidence that, after corrosion of the IrO_2-containing layers, the OER occurs at a totally different, non-active, electrode material (at least a material not containing enough IrO_2 to support adequate electrocatalytic activity).

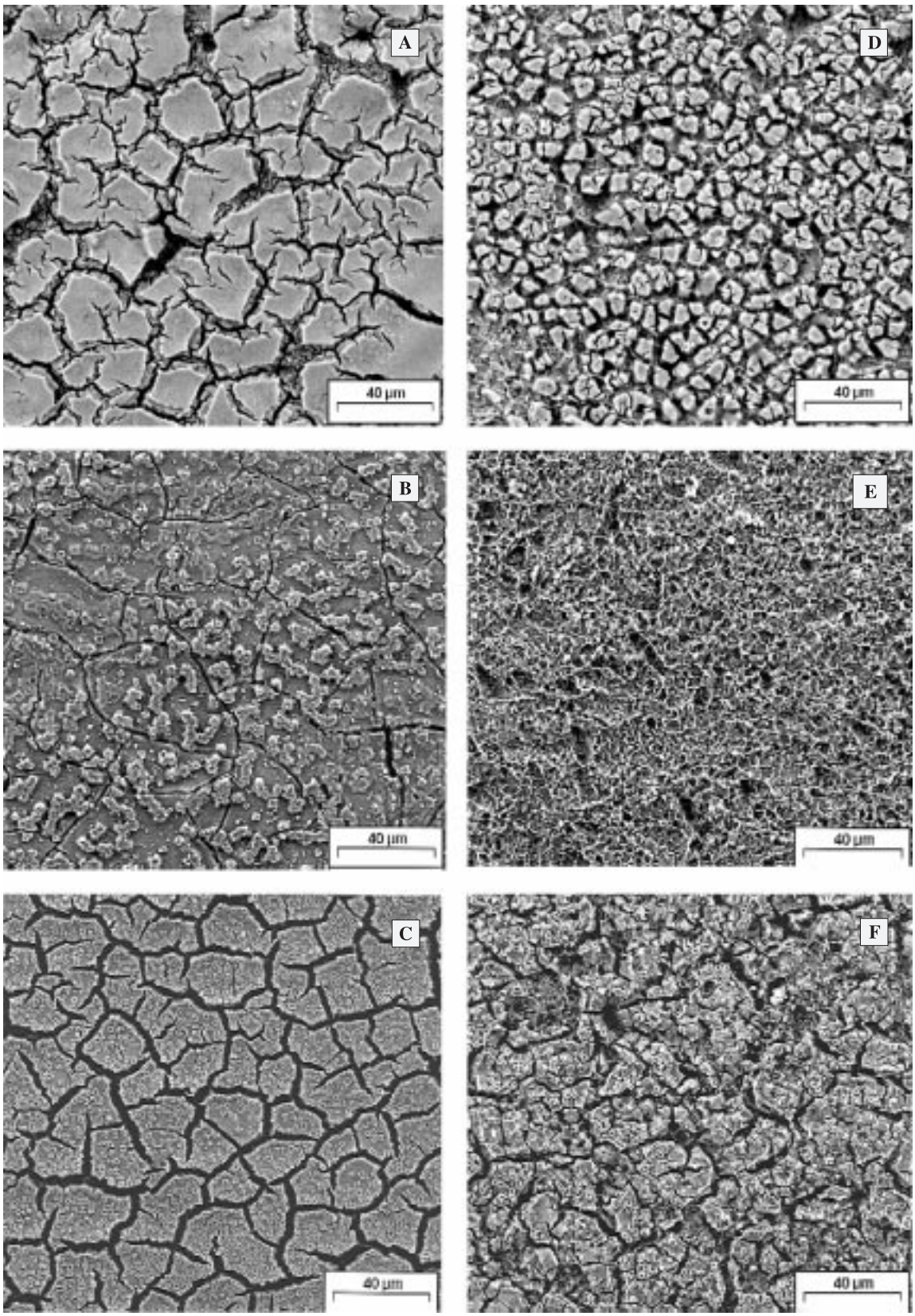

Fig. 12. SEM micrographs of freshly prepared electrodes (a, b, and c) and after accelerated life tests (d, e, and f) in 1.0 mol dm^{-3} $HClO_4$. Nominal electrode composition: $Ir_{0.3}Ti_{(0.7-x)}Sn_xO_2$. (a and d) $x = 0$; (b and e) $x = 0.5$; (c and f) $x = 0.7$.

3.4. *Analysis of the oxide layers by SEM and EDX*

Typical SEM micrographs of the $Ir_{0.3}Ti_{(0.7-x)}Sn_xO_2$ electrodes, before and after the life test, are presented in Figure 12. The behaviour of the SEM and EDX analyses of freshly prepared electrodes have been discussed elsewhere [7].

The SEM micrographs depict a dramatic change in the surface morphology of the electrode after the life test. The morphological aspect of the $Ir_{0.3}Ti_{(0.7-x)}Sn_xO_2$ electrodes after the life test showed a high dependence on the oxide layer composition. Ti-rich electrodes still showed mud-crack morphology, although the crystallites are now of reduced size and countless regions with the Ti-support are exposed to solution (Figure 12d). The EDX analyses of the remaining regions of the oxide layer show low Ir intensity response after total deactivation of the electrodes, without showing a significant increase in the Ti response (Figure 13a and b). These results are consistent with CV and EIS results. Although deactivation of the $Ir_{0.3}Ti_{0.7}O_2$ electrode is influenced by different factors, the corrosion promoted by the slow coating consumption due to oxidation and dissolution of IrO_2 is the main deactivation process of the $Ir_{0.3}Ti_{0.7}O_2$ oxide layer during most of its service life.

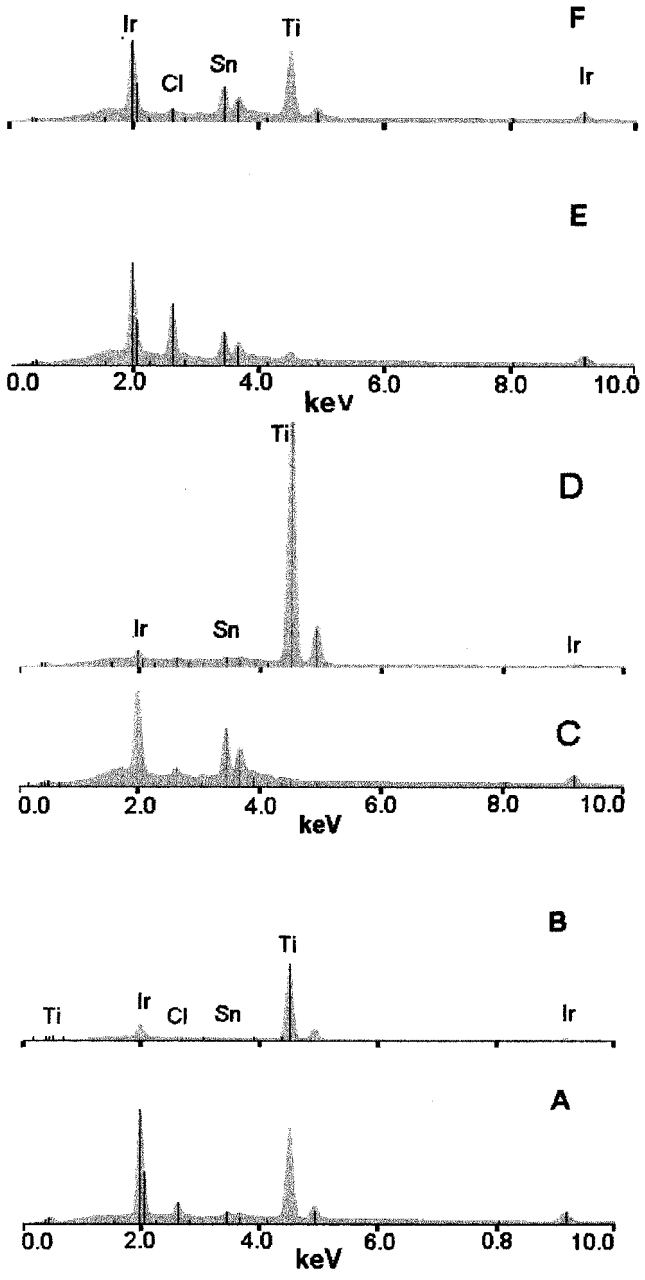

Fig. 13. EDX spectra before (a, c, and e) and after the accelerated life test (b, d, and f) of the nominal electrode composition: $Ir_{0.3}Ti_{(0.7-x)}Sn_xO_2$. (a and b) $x = 0$; (c and d) $x = 0.4$; (e and f) $x = 0.7$.

The replacement of TiO_2 by SnO_2 produced some changes in the deactivation mechanism. Ternary oxide mixtures showed a larger and more damaged oxide layer. The destruction of the oxide layer increased with SnO_2 content. This behaviour is in agreement with the increase in the intensity of the Ti peak observed in the EDX spectra when the SnO_2 content was increased (Figure 13). The 'sponge-like' morphology observed for the $Ir_{0.3}Ti_{0.3}Sn_{0.4}O_2$ electrode resulted from heavy corrosion and erosion of the oxide layer during electrolysis. The EDX spectra showed predominantly Ti peaks with only a small residual signal of Ir after the life test. This behaviour confirmed that IrO_2 was almost completely removed from the oxide layer.

These results are consistent with the decrease in service life observed for the $Ir_{0.3}Ti_{(0.7-x)}Sn_xO_2$ electrodes as a function of composition (Figure 2). The smallest service life was observed for the electrode showing few residual active oxide and almost a complete Ti-support exposure after deactivation (40% SnO_2). These results suggest that for 40–60% SnO_2 content erosion of the oxide layer is the main deactivation process. The partial substitution of TiO_2 by SnO_2 in the oxide layer probably hinders the formation of a solid solution between IrO_2 and TiO_2, limiting the stabilizing action of the later component. The low interaction among the different components leads to the formation of an oxide layer with small particles leading to a high surface area and a high degree of dispersion of the catalytic oxide (IrO_2), but decreasing the mechanical stability of the oxide layer. Erosion is possible, mainly because the coating is porous and gas evolution at the surface is very intense, inducing the detachment of some coating particles.

The complete replacement of TiO_2 by SnO_2 changed the deactivation mechanism. Although the intense O_2 evolution promoted changes in the morphology of the oxide layer, Figure 12 only reveals partial coating consumption after the accelerated life test. This fact was confirmed by comparison of the EDX spectra before and after the accelerated life test. EDX spectrum analysis permits the following observations: (a) the Ti peak showed a significant increase after deactivation; (b) the Ir peak showed a small decrease in intensity; (c) the Cl peak practically disappeared; and (d) the Sn remained unaffected. These results can be understood if we consider that metal base passivation was the main factor responsible for the deactivation of the oxide layer. The overall behaviour of the EDX spectrum after the life test suggests that the rougher external part of the IrO_2-rich active layer is initially destroyed by a combination of erosion and corrosion. The high surface area (see Figure 3 – q_a value for the freshly prepared electrode) and the increase in R_f

over most of the service life agree with a deactivation mechanism promoted by metal base passivation.

4. Conclusions

The deactivation process of $Ir_{0.3}Ti_{(0.7-x)}Sn_xO_2$ electrodes arises from a combination of different factors, such as coating consumption by corrosion, mechanical damage due to intense O_2 evolution and metal base passivation. The overall behaviour of the parameters supplied by EIS, CV, SEM, and EDX analyses made it possible to describe the overall deactivation mechanism as follows: in the first hours of service life, the rougher external part of the layer is destroyed by a combination of erosion and corrosion. Next, the more compact part, still showing excellent catalytic activity, is destroyed mostly by corrosion. During this process the IrO_2-doped TiO_2 interlayer, formed during preparation of the electrode, gradually becomes thicker and less conductive. Finally, when the coating layer is almost totally corroded, a poorly IrO_2-doped TiO_2 layer, grown by oxidation of the Ti-support, becomes the main factor in the complete deactivation the of electrode material. The sudden change in R_f, C_f, and R_{ct} values observed at the end of service life indicates total deactivation of the oxide layer.

The service life showed a dependence on electrode composition. The replacement of TiO_2 by SnO_2 in the $Ir_{0.3}Ti_{0.7}O_2$ electrode leds to a decrease in performance for SnO_2 contents above 30% mol. The contribution of the corrosion, erosion, and passivation phenomena to the global deactivation mechanism is dependent on the electrode composition directly related to morphological factors and an absence of synergetic effects.

Acknowledgements

T.A.F. Lassali wishes to thank FAPESP (Brazil) for a fellowship. L.O.S. Bulhões thanks PADCT/FINEP for financial support. J.F.C. Boodts thanks FAPEMIG/CAPES, for a visiting professor fellowship.

References

1. F. Hine, M. Yasuda, T. Nora, T. Yoshida and J. Okuda, *J. Electrochem. Soc.* **126** (1979) 1439.
2. R. Kotz, H.J. Lewerenz and S. Stucki, *J. Electrochem. Soc.* **130** (1983) 825.
3. Ch. Comninellis and G.P. Vercesi, *J. Appl. Electrochem.* **21** (1991) 335.
4. G.P. Vercesi, J. Rolewicz and Ch. Comninellis, *Thermochim. Acta* **176** (1991) 31.
5. J. Krýsa, L. Kule, R. Mráz and I. Rousar, *J. Appl. Electrochem.* **26** (1996) 999.
6. J. Krýsa and R. Mráz, *Electrochim. Acta* **40** (1995) 1997.
7. T.A.F. Lassali, L.M.C. Abeid, L.O.S. Bulhões and J.F.C. Boodts, *J. Electrochem. Soc.* **144** (1997) 3348.
8. R. Garavaglia, M. Mari and S. Trasati, *Surf. Technol.* **23** (1984) 41.
9. B. Boukamp, 'Equivalent circuits', Twente University, Enschede, The Netherlands, 1989.
10. G. Lodi, E. Sivieri, A. Battisti and S. Trasatti, *J. Appl. Electrochem.* **8** (1978) 135.
11. V.A. Alves, L.A. da Silva and J.F.C. Boodts, *J. Appl. Electrochem.* **28(9)** (1998) 899.
12. S. Trasatti, (Ed.), '*Electrodes of Conductive Metallic Oxides*', Part A, Elsevier, Amsterdam (1980).
13. H. Tamura and C. Iwakura, *Int. J. Hydrogen Eng.* **7** (1982) 857.
14. S-M Lin and T-C Wen, *J. Electrochem. Soc.* **140** (1993) 2265.
15. J. Krýsa, J. Maixner, R. Mráz and I. Rousar, *J. Appl. Electrochem.* **28** (1998) 369.
16. C. Iwakura, K. Hirao and H. Tamura, *Electrochim. Acta* **22** (1977) 329.
17. R. Kötz, S. Stucki, D. Scherson and D.M. Kolb, *J. Electroanal. Chem.* **172** (1984) 211.
18. S. Gottesfeld and S. Srinivasan, *J. Electroanal. Chem.* **86** (1989) 89.
19. R. Kötz, H. Neff and S. Stucki, *J. Electrochem. Soc.* **131** (1984) 72.
20. T.A.F. Lassali, J.F.C. Boodts and L.O.S. Bulhões, *Electrochim. Acta* **44** (1999) 4203.
21. T. Loucka, *J. Appl. Electrochem.* **11** (1981) 143.
22. Y. Matsumoto, T. Tazawa, N. Muroi and E. Sato, *J. Electrochem. Soc.* **133** (1986) 2257.